# Sent2Agri system based crop type mapping in Yellow River irrigation area

**FAN Jinlong[1], DEFOURNY Pierre[2], DONG Qinghan [3], ZHANG Xiaoyu[4], DE VROEY Mathilde[2], BELLEMANS Nicolas[2], XU Qi[1], LI Qiliang[1], ZHANG Lei[4], GAO Hao[1]**

1. *National Satellite Meteorological Center, Beijing* 100081*, China*;
2. *Université catholique de Louvain, Louvain-la-Neuve, Belgium*;
3. *Flemish Institute for Technological Research, Mol, Belgium*;
4. *Ningixa Institute of Meteorological Sciences, Yinchuan* 750000 *China*

**Abstract:** Agricultural monitoring is essential for an adequate management of food production and distribution. Crop land and crop type classification, using remote sensing time series, form an important tool to capture the agricultural production information. The recently launched Sentinel-2 satellites provide unprecedented monitoring capacities in terms of spatial resolution, swath width and revisit frequency. The Sentinel-2 for Agriculture (Sen2Agri) system has been developed to fully exploit those capacities, by providing four relevant earth observation products for agricultural monitoring. Under the Dragon4 Program, the crop mapping with various satellite images and a specific focus on yellow river irrigated agricultural area in the Ningxia Hui Autonomous region in China was carried out with the Sentinel-2 for Agriculture system (Sent2Agri). 9 types of crop were classified and the crop type map in 2017 was produced based on 35 scenes Sentinel 2A/B images. The overall accuracy computed from the error confusion matrix is 88%, which include the cropped and uncropped types. After the removal of the uncropped area, the overall accuracy for cropped decrease to 73%. In order to further improve the crop classification accuracy, training dataset should be further improved and tuned.

**Key words:** Crop Mapping, Dragon Program, Sentinel 2, Sent2Agri system

**Citation format: Fan J L,Defourny P,Dong Q H,Zhang X Y,De Vroey Mathilde,Bellemans Nicolas,Xu Q,Li Q L,Zhang L and Gao H. 2020. Sent2Agri system based crop type mapping in Yellow River irrigation area. Journal of Remote Sensing(Chinese). 24(S1): 10−16**

## 1 Introduction

The world population is growing continuously and imposing the great pressure on our planet's ecosystems. Food production is one of the major components of this pressure. Agricultural monitoring is essential for an adequate management of food production and distribution (Reynolds, et al, 2000; Liu, et al, 2014). Being able to estimate cropped areas and predict crop yields is crucial for decision makers around the globe. Satellites are a valuable resource for obtaining information at a large scale and with a high revisit frequency, which meets two important requirements for agricultural monitoring. Moreover, the timeliness of the information is another crucial concern. The earliest accurate information can be delivered, the most useful it is for decision makers and agriculture producers. In this context agricultural monitoring has become more and more essential (Badhwar et al, 1984; Adamowicz et al., 2005; Poh Sze Choo et al., 2005; Feng et al., 2010; Sakamoto et al, 2014). Nowadays, several international initiatives has set up to provide local and global agricultural monitoring, of which one of the most important efforts has been GEO's Global Agricultural Monitoring (GEOGLAM) Initiative (Becker-Reshef et al., 2010).

Crop land and crop type classification, using remote sensing time series, form an important tool, among others, to deliver such information. A large variety of crop mapping methods at different scales and showing various levels of accuracy can be found in the literature (Lunetta et al., 2004; Carrão et al., 2008) . From the first use of satellites for agricultural monitoring in the 1970's (Marvin E. Bauer et al., 1979) to the latest study, crop mapping strategies have evolved tremendously. Methods have been adapted continuously, to the increasing performances of embarked sensors and to increasing computational capacities. A first main challenge of crop mapping is to differentiate annual cropland from other land uses and especially from other green land covers. Working with time series instead of single date images allows extracting temporal features, which are a great asset for classifying cropland and identifying different crop types (Osman et al., 2015; Gómez et al., 2016; Xiong et al., 2017). Another great issue is the spatial resolution. Often, sensors with a high revisit frequency and a large swath width offer a coarser spatial resolution. Using such sensors to map heterogeneous agricultural areas is problematic when the field areas are inferior to the sensor's pixel size, causing mixed pixels.

The recently launched Sentinel-2 satellites provide unprecedented monitoring capacities in terms of spatial resolution, swath width and revisit frequency (ESA, 2015; Martins et al., 2017; USGS, 2017). With its swath width of 290 km and 10m spatial resolution,

**Received:** 2019-10-21; **Accepted:** 2020-04-16

combined with its 5 days revisit frequency, the constellation of two satellites presents a great potential for large scale crop mapping with high precision and accuracy. The Sentinel-2 for Agriculture (Sen2Agri) system (Sentinel-2 for Agriculture, 2015; Orfeo ToolBox, 2015; ESA, 2015) , a project funded by the European space agency and led by Université Catholique de Louvain (UCL), has been developed to fully exploit those capacities, by providing four relevant earth observation products for agricultural monitoring. The system can provide a monthly cloud free image composite, a binary cropland mask differentiating cropland from other land covers, a crop type map, classifying the main crops of a region and a vegetation status map with LAI or NDVI values (Inglada et al., 2015; Matton et al., 2015; Valero et al., 2016).

Under the Dragon4 Program, the crop mapping with various satellite images and a specific focus on yellow river irrigated agricultural area in the Ningxia Hui Autonomous region in China was carried out with the Sentinel-2 for Agriculture system (Sent2Agri). This paper presents the results and the performance evaluation of Sent2Agri in this area.

## 2 Study area and Data

### 2.1 Study area

The northern part of the Ningixa yellow river irrigation area was selected as the study area in this paper. The Ningxia Hui autonomous region is a 66.400 km² area in Northwest China. Amongst 6 million people living in the region, 66.4% is the rural population. In 2016, the farmland represented 1.2921 million ha, including 501, 364 ha of irrigated crops and 781,721 ha of rain-fed crops (Ningxia Statistics Bureau, 2017). Since 1985, the Ningxia Hui region has been self-sufficient in terms of food supply and even developed from an import province to an export province. The main crops in Ningxia are grains, oil plants, vegetables, and pasture grass. Grains account for the largest farmland surface, namely 59% of the total farmland. Those grains are mainly wheat, rice, corn and minor crops (peas, horse beans, haricot beans, grass peas, buckwheat, glutinous millet and millet etc.). The latter are mostly produced in the southern mountainous and central arid areas.

The Ningxia region is naturally divided in 3 geomorphic and economic zones (NERC, 2008). The mountainous and loess hilly district (MLHD) in the south, the centrally located dry and desertified district (DDD) and the Yellow River irrigated district (YERID) in the northern plains. Geology and climate vary tremendously, from the south to the north. The topography declines, the temperature rises, and the precipitation decreases. These gradients cause 3 different agricultural landscapes. In the MLHD 70% of the cultivated land consists of slope farmlands. Although this region has the highest precipitation, the hilly landscape and the uneven temporal distribution of rainfall hinder most agricultural activities. The DDD, as its name indicates, is a very arid area, mostly covered by grassland (77% of Ningxia's grasslands). It is however suited for Yellow river irrigation, given its proximity to the water body and its flat topography. The YERID is the most important rural part of Ningxia. It represents only one third of the total farmland in the region, but accounts for two thirds of Ningxia's grain production and agricultural production value. YERID's Gross Domestic Product represents almost 90% of the region's total. Annual rainfall is extremely low in this area, but the Yellow River allows an efficient irrigation of the fields. In YERID, wheat, rice and corn are by far the major crops at present. This study was focused on the YERID, as it is the most important agricultural district of the whole region. The study area corresponds to six Sentinel-2 tiles (Fig. 1).

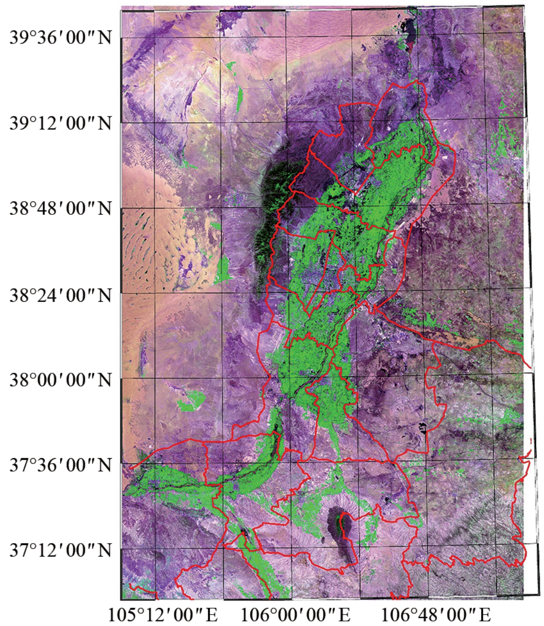


Fig.1 The main study area

### 2.2 Sentinel-2 Data

The Sentinel satellites are part of European Space Agency's Copernicus program. Sentinel-2A was launched in June 2015 and complemented by Sentinel-2B in March 2017. This second Sentinel mission is equipped with high resolution multispectral (MS) sensors, providing information on land surface and vegetation for instance. Sentinel-2 provides an unprecedented 10 m spatial resolution with a 5 days global revisit frequency, a 13 bands imager and a 290 km swath width. Table 1 lists the spectral and spatial specifications of the Sentinel 2A/B.

Through the Sen2Agri system, Sentinel-2 L1C (top of atmosphere) images were automatically downloaded for the six tiles covering the study area and over the whole 2017 growing season from the Copernicus Open Access Hub(https://scihub. copernicus. eu/). Using Sen2Agri's L2A processor, a Multi-sensor Atmospheric Correction and Cloud Screening (MACCS algorithm) was performed on the top of atmosphere images, resulting in an L2A time series of 27 Sentinel-2 A (S2A) and 8 Sentinel-2 B (S2B) images between December 8, 2016 and November 1, 2017 (Fig. 2). Fig.3 shows the availability of cloud free images over the study area.

### 2.3 Field data

The reference data needed for training and validation of the classification was collected through field observations. Reference points were gathered using GPS cameras and processed via a Quick Photo Data Processor. The method implies two major steps. First georeferenced pictures were taken with a GPS camera along the study area's roads following a predefined itinerary. In a second phase, land cover and crop type classes were retrieved by screening the pictures with the processor. The final product of this process is a table file gathering all GPS points with corresponding classes, author, roadside (left or right), collecting dates and times and the corresponding image file names.

**Table 1 Spatial resolution Bands and associated Signal to Noise ratio (SNR)**

| Band number | Central wavelength/nm | Bandwidth/nm | Lref (reference radiance)($W\ m^{-2}\ sr^{-1}\ \mu m^{-1}$) | SNR @ Lref | Resolution/m |
|---|---|---|---|---|---|
| 1 | 443 | 20 | 129 | 129 | 60 |
| 2 | 490 | 65 | 128 | 154 | 10 |
| 3 | 560 | 35 | 128 | 168 | 10 |
| 4 | 665 | 30 | 108 | 142 | 10 |
| 5 | 705 | 15 | 74.5 | 117 | 20 |
| 6 | 740 | 15 | 68 | 89 | 20 |
| 7 | 783 | 20 | 67 | 105 | 20 |
| 8 | 842 | 115 | 103 | 172 | 10 |
| 8a | 865 | 20 | 52.5 | 72 | 20 |
| 9 | 945 | 20 | 9 | 114 | 60 |
| 10 | 1375 | 30 | 6 | 50 | 60 |
| 11 | 1610 | 90 | 4 | 100 | 20 |
| 12 | 2190 | 180 | 1.5 | 100 | 20 |

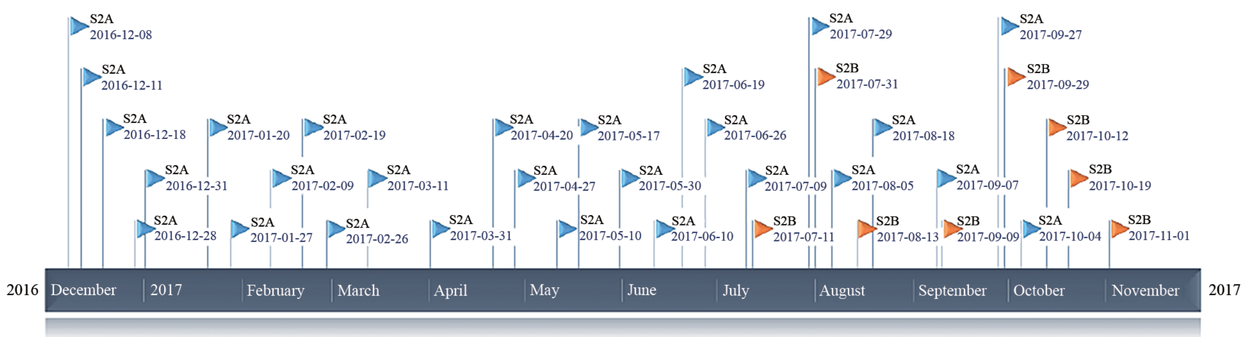


Fig.2 Sentinel 2 satellite images acquired for this study

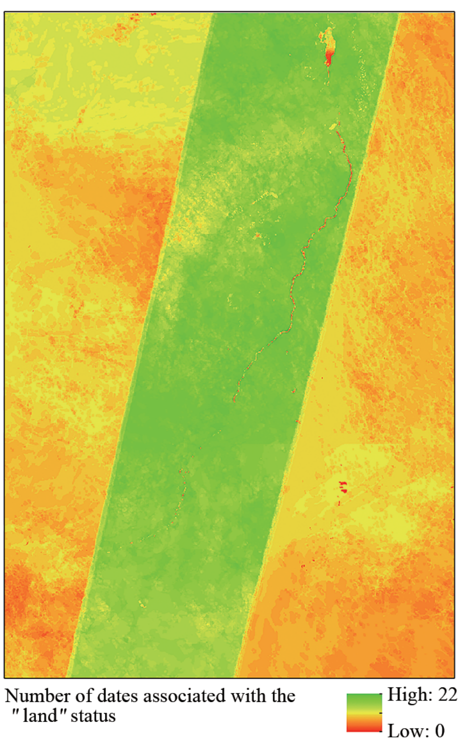


Fig.3 Cloud free images count over the study area

A field campaign was carried out in June 2017, providing about 1500 ground truth points with spatial reference and associated crop or other land cover classes. Those sample points are distributed over the irrigated area as shown on Figure 4. Based on those points and using Google Earth as visual reference, polygons were created, covering the plot extents, to increase the number of reference pixels per class. In addition, the in-situ dataset was complemented by delineating additional non-cropland samples to cover the whole range of landscape diversity. The dataset was randomly divided into training and validation subset, each containing 50% of the initial dataset. As a result, samples of most classes are more or less equally distributed between the two subsets. Table 2 shows the number of polygons and estimated number of pixels per class in the training and validation datasets.

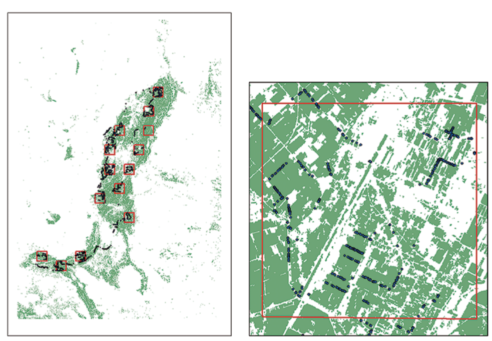

Fig.4 In-situ sample points distribution in the study area

**Table 2 Training and validation data-sets for 2017 growing season**

| | | Samples | | Pixels (10 m) | |
|---|---|---|---|---|---|
| | Land Cover | Training | Validation | Training | Validation |
| Crops | fodder | 19 | 39 | 433 | 1054 |
| | Wheat | 40 | 41 | 1241 | 1274 |
| | Rice | 121 | 111 | 3983 | 3697 |
| | Corn | 101 | 92 | 3925 | 3698 |
| | Grapes | 25 | 38 | 1397 | 2028 |
| | Cabbage | 8 | 12 | 208 | 336 |
| | Tomatoes | 3 | 4 | 53 | 70 |
| | Watermelons | 3 | 4 | 86 | 136 |
| | Medlar | 3 | 5 | 106 | 242 |
| No crops | Plantations | 67 | 60 | 2964 | 2273 |
| | Grassland | 6 | 5 | 7068 | 4700 |
| | Forests | 11 | 9 | 4054 | 1883 |
| | Bare Soils | 33 | 42 | 1576 | 5081 |
| | Build-up | 90 | 74 | 5167 | 5081 |
| | Water bodies | 43 | 35 | 3367 | 1904 |
| | Total | 573 | 571 | 35628 | 34424 |

## 3 Methods

### 3.1 Approach of the Sent2Agri System

The unprecedented capacities of Sentinel-2 satellites are an important asset in many fields, and particularly in agricultural monitoring. The 10 m spatial resolution facilitates the generation of crop maps on field level. Sent2Agri system, an open source time series processing chains for large-scale production, aims to fully exploit those new Sentinel-2 capacities. The final approach of the Sent2Agri System was tested through the following studies. Inglada et al. (2015) concluded Sentinel-2 will certainly bring improvements in the results thanks to the enhanced spatial resolution and the increased number of spectral bands, mainly in the red-edge spectrum. Matton et al. (2015), proposes and demonstrates an automated methodology for annual cropland mapping performing along the season in various agricultural systems using high spatial and temporal resolution remote sensing time series. Valero et al. (2015) developed a method to create a dynamic binary cropland mask that will be used as input data for the crop type map and crop status map.

The workflow (Fig. 5) of the Sen2Agri's for the cropland map and the crop type map production is described in the Seninel-2 Agriculture Software User Manual (Udroiu et al., 2017). The processing chain of the crop type map is also based on a random forest classifier. The values of the parameters for the random forest classifier were kept default (100 trees, maximum depth 25 and 25 features at each node). The main inputs are the bottom of atmosphere Sentinel-2 images and in situ data representing all the expected crops of the study area. Moreover, the cropland mask generated for the same period is also needed as input. The L2A images are linearly interpolated to obtain smooth time series and a temporal resampling ensures a homogeneous distribution of the data over time. The features extracted for the random forest classifier are surface (TOC) reflectance, NDVI, NDWI and brightness, which were defined as most pertinent by Inglada et al. (2015). The classification model is then used to classify the cropland area, as defined by the cropland mask. The cropland mask production is based on a random forest classifier. The input reference data can be in situ data, collected and provided by the user, or a reference raster land cover map, which is the CCI Land Cover 2015 product by default, but can be provided by the user as well (Udroiu et al., 2017). A first crop type map was generated using the imagery of the whole growing season and the 2017 *in situ* training dataset, representing 9 different crops. Crop mask was used as input for this crop type map. The crop type map production workflow is schematized in Fig. 5.

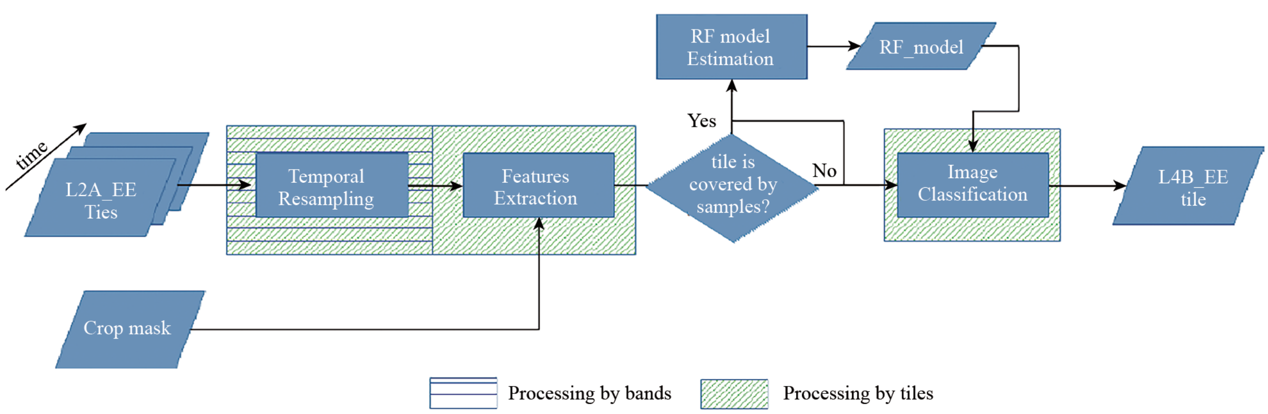


Fig.5 Workflow of the Sent2Agri for the Crop Type Classification

### 3.2 Validation methods

In this study the validation of the generated maps was carried out independently, outside the Sen2Agri system, using the validation subset of the reference data. To evaluate and compare the performances of the Sen2Agri system, a conventional validation method was used, computing performance metrics such as the F1-scores and the overall accuracy. Those metrics are based on an error confusion matrix between the classified pixels and reference validation pixels. The reference pixels were obtained from the validation set of in situ polygons selected earlier. Two validation datasets were generated, one binary raster differentiating "cropland" and "no cropland" for the cropland masks validation and another featuring the different crops for the crop type map validation. The error confusion matrices were computed as presented in Table 3 and the performance metrics were calculated with the equation 1—4. Table 3 shows the typical format of a confusion matrix, where $n_{ij}$ is the number of observations categorized as $i$ in the reference dataset and as $j$ in the predicted crop map and $J$ is the number of different classes.

**Table 3 Typical Error confusion matrix**

| | | Classified | | | |
|---|---|---|---|---|---|
| | | $j = 1$ | $j = 2$ | … | $j = J$ |
| Reference | $i = 1$ | $n_{11}$ | $n_{12}$ | | $n_{1J}$ |
| | $i = 2$ | $n_{21}$ | $n_{22}$ | | $n_{2J}$ |
| | … | | | | |
| | $i = J$ | $n_{J1}$ | $n_{J2}$ | | $n_{JJ}$ |

From the error confusion matrix, several performance metrics can be derived. The most common and simple ones are the F1-scores and the overall accuracy. The F1-score (Eq. 3) is derived from the precision and the recall for each class, which are computed through Eq. 1 and 2 respectively. It gives an indication of the classification performance per class.

$$\text{Precision} = \frac{n_{ii}}{\sum_{j=1}^{J} n_{ij}} \tag{1}$$

$$\text{Recall} = \frac{n_{jj}}{\sum_{i=1}^{J} n_{ij}} \tag{2}$$

$$\text{F1} - \text{score} = 2 * \frac{\text{Precision} * Recall}{\text{Precision} + Recall} \tag{3}$$

The overall accuracy gives the proportion of observations classified correctly. It can be computed through Eq. 4.

$$\text{Overall Accuracy} = \frac{\sum_{i=1}^{J} n_{ii}}{\sum_{i=1}^{J} \sum_{j=1}^{J} n_{ij}} \tag{4}$$

## 4 Results

### 4.1 Crop type map and error evaluation

The crop type map generated with the Sen2Agri system, based on the previously obtained cropland mask, using images of the whole 2017 growing season and the *in-situ* training dataset, is shown in Fig. 6. From a visual analysis of the full extent, the main crops, namely maize and rice clearly stand out followed by wheat. Those three main crops are indeed the major crop types grown in this region. Based on a closer look on the plots, rice and maize seem to be well distinguished from one another, while maize and wheat appear to be mixed inside some plots. Generally, there is an undeniable salt and pepper effect, due to the pixel-based approach.

To assess the quality of the classification, an error confusion matrix was generated between the crop type map and the in-situ validation dataset containing each crop type, and quality metrics were computed (Table 4). Several observations can be made, based on the confusion matrix and the performance metrics. First, the overall accuracy computed from the confusion matrix is 88%, which seems high. However, as the "no crop" pixels are numerous, they weigh a lot in the overall accuracy. It is therefore interesting to calculate the overall accuracy of the crop type classification only, excluding the "no crop" pixels. The result (73%) is significantly lower, meaning the cropland mask contributes largely to the overall accuracy of the crop type map. The real accuracy of the crop type classification is however 73%. Secondly, when analyzing the individual performances for each class, certain crops clearly stand out in terms of classification accuracy. Rice was classified with high accuracy (89% F1-score). It was barely confused with other crops, meaning its spectral signature and its temporal features are very specific and different from other crops. Fodder was also classified quite accurately (85% F1-score). Other crops, like maize, wheat, grapes or cabbage have lower F1-scores, ranging from 61% (wheat and grapes) to 77% (maize). Those crops seem to be less distinguishable. Wheat and grapes were confused with maize quite often. Other land covers ("no crop") were misclassified as maize as well. Another notable error is the confusion between grapes and other land covers, probably bare soil. Finally, it is clear the minor classes have been completely misclassified or overlooked by the classification model. They have not once been classified correctly. While the main and minor crops show very high F1-scores, the three minor crop types score 0 in both precision and recall. This is majorly due to their poor representation in the training dataset, compared to other classes. In a random forest classifier, each tree uses a subset of the total set of features to define decision rules for each node. As a result, classes that are poorly represented in the complete training dataset have a smaller chance to be represented in the feature subset for each tree. At the end, when performing the majority voting, those classes tend to be overlooked. A potential solution to tackle the issue of the minor classes was to gather the three minor classes in one "other" class for the main classification, to perform a separate classification with only those three classes and then substitute the "other" class with the separate minor classification.

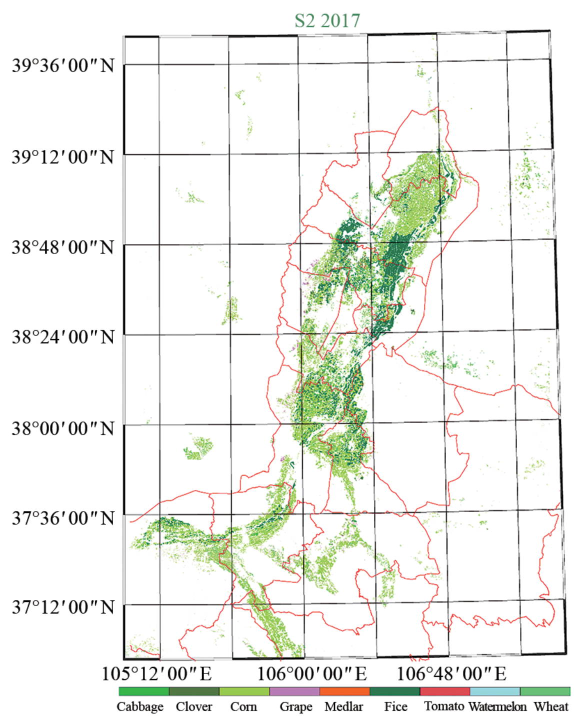


Fig.6 Crop type map for the irrigation area in 2017

**Table 4 The error confusion matrix**

| | | Classified | | | | | | | | | | |
|---|---|---|---|---|---|---|---|---|---|---|---|---|
| | | Fodder | Wheat | Maize | Rice | Grape | Cabbage | Tomato | Watermelon | Medlar | No Crop | Precision |
| Ground Truth | Fodder | 815 | 3 | 17 | 22 | 0 | 2 | 0 | 1 | 0 | 60 | 0.89 |
| | Wheat | 16 | 678 | 22 | 114 | 29 | 6 | 0 | 0 | 6 | 298 | 0.58 |
| | Maize | 45 | 264 | 3170 | 184 | 294 | 84 | 56 | 10 | 29 | 259 | 0.72 |
| | Rice | 89 | 12 | 196 | 3334 | 0 | 13 | 4 | 0 | 0 | 44 | 0.90 |
| | Grape | 2 | 17 | 21 | 0 | 942 | 0 | 0 | 1 | 3 | 755 | 0.54 |
| | Cabbage | 2 | 2 | 1 | 0 | 0 | 214 | 0 | 48 | 0 | 17 | 0.75 |
| | Tomato | 25 | 0 | 1 | 0 | 0 | 0 | 0 | 0 | 0 | 10 | 0.00 |
| | Watermelon | 0 | 0 | 9 | 0 | 0 | 0 | 0 | 0 | 0 | 76 | 0.00 |
| | Medlar | 0 | 0 | 1 | 0 | 8 | 0 | 0 | 0 | 0 | 204 | 0.00 |
| | No Crop | 6 | 84 | 387 | 114 | 58 | 35 | 0 | 0 | 4 | 21201 | 0.00 |
| | Recall | 0.82 | 0.64 | 0.83 | 0.88 | 0.71 | 0.60 | 0.00 | 0.00 | 0.00 | 0.92 | |
| | F1-Score | 0.85 | 0.61 | 0.77 | 0.89 | 0.61 | 0.67 | 0.00 | 0.00 | 0.00 | 0.95 | |

### 4.2 Crop land and error evaluation

The cropland mask was generated using Sentinel-2 imagery from the start till the end of season, implying 24 dates and with the in-situ training dataset. The resulting cropped land mask is shown in Fig. 6 as well. Visually, this cropland mask seems very satisfying, as the whole irrigated agricultural area seems to be classified correctly as "crop". The main built up areas and the yellow river are clearly distinguishable as "no crop". When comparing the zoomed in section to the equivalent Sentinel-2 composite image, the smaller and more scattered built up areas, the narrow roads and even boundaries between different plots seem to be classified quite accurately as "no crop". Due to the pixel-based approach, however, a slight salt and pepper effect is almost unavoidable.

Statistically, and according to the in-situ validation dataset, the high accuracy of this cropland mask is confirmed. The F1-scores of "crop" and "no crop" are 92% and 94% respectively and the overall accuracy is 93%.

## 5 CONCLUSION

Under the Dragon Program, a joint collaborative study for crop mapping with the Sent2Agri system was carried out successfully in the yellow river irritation area in Northwest Ningxia Hui autonomous region. The satellite data collecting and processing were fully benefited from the Sent2Agri system. The classifier and the parameters setting were used the default values of the Sent2Agri system. As the key of the remote sensing classification, the scheme of field data collection and the training dataset development and tuning were performed by the both teams. The result demonstrated the good performance of Sent2Agri system firstly in the fully irrigated area in the world. 9 types of crop were classified and the crop type map in 2017 was produced based on 35 scenes Sentinel 2A/B images. The overall accuracy computed from the confusion matrix is 88%, which include the cropped and uncropped types. After the removal of the uncropped area, the overall accuracy for cropped only decreases to 73%. The major crop types, like rice was classified with high accuracy with 89% F1-score. Fodder was also classified quite accurately (85% F1-score). Other crops, like maize, wheat, grapes or cabbage have lower F1-scores, ranging from 61% (wheat and grapes) to 77% (maize). Those crops seem to be less distinguishable. It is clear the minor classes have been completely misclassified or overlooked by the classification model. In order to further improve the crop classification accuracy, more field visits should be arranged and the training dataset of each type of crop should be balanced statistically and spatially.

In addition to the agricultural production management, the classified image is helpful for the other agriculture related sectors. The irrigation management is of very importance in this region. The water needs and water use efficient of the region will be calculated with crop type map in order to improve the water managements. The precision agricultural-meteorological service requires the crop type maps in the region as well and then the agro-meteorological forecast for the crop growth stage may be improved. The early warning of agricultural meteorological disaster for the concrete crop type may be provided precisely. With the implementation of this dragon project, the crop type mapping practice is expected to be further improved and the users may be easily benefited from the Sent2Agri system.

## REFERENCES

Badhwar, G. B. Automatic corn-soybean classification using Landsat MSS data. II. Early season crop proportion estimation. Remote Sensing of Environment, 14, 31 – 37 (1984).

Carrão H., Gonc¸ alves P., Caetano M., 2008. Contribution of multispectral and mul-titemporal information from MODIS images to land cover classification. RemoteSens. Environ. 112 (3), 986 – 997.

ESA Sentinels—Sentinel-2: Operations Ramp-up Phase. Available online: https://sentinel.esa.int/web/sentinel/missions/sentinel-2/operations-ramp-up-phase (accessed on 21 August 2015).

ESA.Sentinel-2 User Handboos[M].ESA, 2015.

Fan X S,Xu W B and Fan J L. 2015.Mapping winter wheat growing areas in the North China Plain with FY-3 250 m resolution data. Journal of R emote Sensing,19( 4) : 586 — 593[DOI: 10. 11834 / jrs. 20154135]

Gómez C., White J.C., Wulder M. A., 2016, Optical remotely sensed time series data for land cover classification: A review, ISPRS Journal of Photogrammetry and Remote Sensing, 116, 55-72.

Jinlong F. and Mingwei Z. (2012). Supporting Agricultural Monitoring in APEC with FengYun Satellite data. Workshop on the application of Remote Sensing and GIS on Crops Productivity among APEC Economies, Beijing, China, 30-31 July 2012.

Jinlong Fan. Updates on the FY-3 MERSI satellite data processing and delivering[M]. SIGMA project annual meeting 2015, Brussels, Belgium, 2015, 11

Liu, M.W.; Ozdogan, M.; Zhu, X. Crop type classification by simultaneous use of satellite images of different resolutions. IEEE Trans. Geosci. Remote Sens. 2014, 52, 3637–3649.

Lunetta R.S., Johnson D.M., Lyon J.G., Crotwell J., 2004. Impacts of imagery temporalfrequency on land-cover change detection monitoring. Remote Sens. Environ. 89(4), 444–454.

RastM., BezyJ. L., BruzziS.. The ESA Medium Resolution Imaging Spectrometer MERIS a review of the instrument and its mission [J]. International Journal of Remote Sensing, 1999, 20(9): 1681-1702

Martins V.S.; Barbosa C.C.F.; de Carvalho L.A.S.; Jorge D.S.F.; Lobo F.L.; Novo E.M.L.M. Assessment of Atmospheric Correction Methods for Sentinel-2

MSI Images Applied to Amazon Floodplain Lakes. SensRemote. 2017, 9, 322.

Marvin E. Bauer, Jan E. Cipra, Paul E. Anuta, Jeanner B. Etheridge, 1979, Identification and Area Estimation of Agricultural Crops by Computer Classification of LANDSAT MSS Data, Remote Sensing of Environment, 8, 77-92.

NERC,ESRC and DFID, 2008, China Ecosystem Services and Poverty Alleviation Situation Analysis and Research Strategy- Ningxia Case Study

Ningxia Statistics Bureau, 2017, Ningxia Statistical Yearbook, China Statistics Press

ToolBoxOrfeo. Available online: https://www.orfeo-toolbox.org/ (accessed on 21 August 2015).

Osman J., Inglada J., Dejoux J.-F., 2015, Assessment of a Markov logic model of crop rotations for early crop mapping, Computers and Electronics in Agriculture 113, 234-243.

Reynolds C.A.; Yitayew M.; Slack D.C.; Hutchinson C.F.; Huete A.; Petersen M.S. Estimating crop yields and production by integrating the FAO crop specific water balance model with real-time satellite data and ground-based ancillary data. Int. J. Remote Sens. 2000, 21, 3487–3508.

Sakamoto, T., Gitelson, A. A. & Arkebauer, T. J. Near real-time prediction of U.S. corn yields based on time-series MODIS data. Remote Sens. Environ. 147, 219–231 (2014.

Sentinel-2 for Agriculture. Available online: http://www.esa-sen2agri.org/ (accessed on 18 September 2015).

USGS (2017) Landsat missions. United States Geological Survey.

Xiong J., Thenkabail P.S., Gumma M.K., Teluguntla P., Poehnelt J., Congalton R.G., Yadav K., Thau D., 2017, Automated cropland mapping of continental Africa using Google Earth Engine cloud computing, ISPRS Journal of Photogrammetry and Remote Sensing, 126, 225–244.